Structural, optical and electronic properties of a Mg incorporated GaN nanowall network†

Sanjay Kumar Nayak, [a] Mukul Gupta[b] and S. M. Shivaprasad*[ac]

We report the growth of a Mg incorporated GaN nanowall network (NwN) by using a plasma assisted molecular beam epitaxy (PA-MBE) system that was characterized by photoluminescence (PL) spectroscopy, Raman spectroscopy, high-resolution X-ray diffraction (HR-XRD), X-ray photoelectron spectroscopy (XPS) and secondary ion mass spectroscopy (SIMS). We record a PL enhancement (≈ 3.2 times) in nominally and moderately Mg incorporated GaN compared to that of an undoped NwN. Two distinct (and broad) blue luminescence peaks appear at 2.95 and 2.70 eV for the heavily Mg incorporated (10^{20} atoms per cm^3) GaN, of which the 2.95 eV peak is sensitive to annealing. The incorporated Mg concentration is estimated to be 10^{20} atoms per cm^3 while retaining its band edge emission at ≈ 3.4 eV. XPS valence band spectra shows a shift in the Fermi level towards Valence Band Maximum (VBM) and the increase in Mg flux confirms the formation of p-type GaN. Mg accumulation at the nanowall surface and the GaN/Al_2O_3 interface was observed from SIMS measurements.

1 Introduction

Gallium nitride (GaN) is one of the most preferred semiconductor materials for light-emitting diodes (LEDs),[1] high electron mobility transistors (HEMT),[2] lasers,[3] dilute magnetic semiconductors (DMS),[4] solar cells,[5,6] photo electrochemical water splitting,[7] biosensors,[8] and space applications.[9,10] Such widespread applications of GaN are due to its direct band gap, band gap tunability,[11] high mobility, chemical and thermal stability and better internal quantum efficiency[12] for light emission compared to other semiconducting materials such as GaAs and ZnO. Despite great progress in the synthesis of high quality thin films with low dislocation density, the overall efficiency of GaN-based LEDs remains low due to lower light extraction efficiency (LEE) which is caused by a large mismatch in refractive indices between GaN and the ambient.[13] Several methods have been proposed[14–16] to enhance the light extraction efficiency of these materials, among which the use of nanoporous[17,18] structures has shown great promise. Generally, the synthesis of porous structures is achieved by chemical or ion bombardment etching, which unfortunately is prone to introduce defects and impurity states in the material, leading to degradation of crystal integrity and device performance. Thus,

fabrication of the porous structure was achieved using a bottom-up approach, by controlling the kinetics of growth to avoid such pitfalls. Previously, we have shown that, by controlling growth parameters such as substrate temperature and III–V ratio, the GaN NwN can be formed directly on *c*-plane sapphire.[19,20] We have reported that the NwN exhibits superior structural and optical properties compared to that of flat GaN thin films. Our experimental and simulated, based on finite difference time domain (FDTD), findings showed that the observed high PL intensity from GaN NwN is not only due to dislocation filtering but also due to the geometry of its unique surface morphology, which facilitates the reduction in total internal reflection.[21]

It is well known that n-type GaN can be obtained more easily than p-type GaN. Magnesium (Mg) is the most successfully used dopant to make p-type GaN. Mg substitutes Ga in the GaN lattice resulting in an acceptor state in its electronic structure. However, the higher ionization energy (≈ 200 meV) of Mg[22] and the high unintentional n-doping of intrinsic GaN makes it difficult to obtain p-doped GaN. Thus, a very high concentration of Mg ($>10^{20}$ cm^{-3}) is required[23] for obtaining significant and useful p-doping. Typical Mg dopant concentrations between 10^{17} and 10^{19} cm^{-3} have been incorporated in planar GaN films,[24,25] while higher Mg incorporation has been observed to form defects such as N-vacancies, Mg-interstitials, and $Mg_{Ga}V_N$-like clusters. In addition, there can be polarity inversion in the film that can also lead to the degradation of its crystal structure, which results in poor optical properties. Moreover, these defects and complexes may result in self-compensation in p-GaN.[26,27] Experiments based on X-ray photoelectron spectroscopy (XPS) and secondary ion mass spectroscopy (SIMS) measurements of a GaN flat film show that the concentration of Mg incorporated

[a]Chemistry and Physics of Materials Unit, Jawaharlal Nehru Centre for Advanced Scientific Research (JNCASR), Bangalore-560064, India. E-mail: smsprasad@jncasr.ac.in

[b]UGC-DAE Consortium for Scientific Research, Khandwa Road, Indore-452017, India

[c]International Centre for Materials Science, Jawaharlal Nehru Centre for Advanced Scientific Research (JNCASR), Bangalore-560064, India

† Electronic supplementary information (ESI) available. See DOI: 10.1039/c7ra02315d

Paper

on the surface is higher than in the bulk,[28–31] suggesting that GaN with higher surface area may enable higher incorporation of Mg. Since the NwN with its porous structure has a very high surface to volume ratio, it may be a potential candidate for achieving higher incorporation of Mg. In this report we study the effect of incorporation of different quantities of Mg on morphology, crystal structure and optical properties of the GaN NwN.

2 Experimental details

The GaN NwN films were grown on the bare c-plane of sapphire (α-Al$_2$O$_3$) under nitrogen rich conditions by using a radio frequency plasma assisted molecular beam epitaxy system (RF-PAMBE, SVTA-USA) operating at a base pressure of 3×10^{-11} Torr. The detailed procedure of the substrate preparation can be found elsewhere.[32] The temperature of the gallium (Ga) effusion cell was kept at 1030 °C. A constant nitrogen flow rate of 8 sccm (standard cubic centimeter per minute), substrate temperature of 630 °C, plasma forward power of 375 W and growth duration of 4 hours were maintained for all of the films. Mg flux was varied by adjusting the Mg K-cell temperature from 300 °C to 360 °C in steps of 20 °C. The flux values of Mg and Ga were obtained from the beam equivalent pressure (BEP) and are tabulated in Table 1. Surface structural evolution was monitored *in situ* by reflection high energy electron diffraction (RHEED) and the morphology was determined *ex situ* using a field emission scanning electron microscope (FESEM). The structural quality of the films was determined using a high-resolution X-ray diffractometer (HR-XRD, Discover D8 Bruker) with a Cu K$_\alpha$ X-ray source that had a wavelength of 1.5406 Å. The optical properties of the films were studied by photoluminescence spectroscopy (PL, Horiba Jobin Yvon) using a xenon lamp source and 325 nm excitation. Raman spectroscopy with an Ar laser of wavelength 514 nm was performed in the back scattering geometry. Quantification of Mg incorporated in the film was done by *ex situ* X-ray photoelectron spectroscopy (XPS) using an Omicron EA 125 spectrometer and Al-K$_\alpha$ (1486.7 eV) source which had a relative composition detection better than 0.1%. Before performing XPS measurements, GaN NwN films were sputter cleaned by optimized low energy (0.5 keV, 2 μA) Ar$^+$ ions to remove physisorbed adventitious carbon and oxygen without affecting the crystalline quality and composition of the film. The depth dependence of the Mg distribution has been studied by secondary ion mass

spectroscopy (SIMS) using an O^{2+} ion beam of 3 keV with a spot size of 100 μm, rastered over a 5 mm × 5 mm area.

3 Results and discussion

In our previous study we have shown that the unique topography of the GaN NwN structure results in superior optical properties.[21] In the present study we control Mg incorporation in the NwN while the Mg : Ga ratio was changed in the range of 0.0017 < Mg : Ga < 0.1102. The surface morphology of the grown films obtained by FE-SEM imaging have similar morphology that is independent of the amount of Mg incorporation. The average pore dimension of all of the films is in the range of 200 ± 20 nm. The typical SEM image of sample E (grown with maximum Mg flux rate) is shown in the inset in Fig. 1 (all FE-SEM images are provided in Fig. 1 in the ESI†).

PL and Raman spectroscopy techniques have been extensively employed in the past to study the effect of Mg incorporation on the optical properties of GaN.[33–36] In the literature, commonly observed luminescence peaks of Mg doped GaN appear at ≈ 3.27 eV due to the DAP transition for moderately Mg incorporated (Mg concentrations of less than 10^{19} atoms per cm^3) samples and a broad ≈ 2.7–2.9 eV blue luminescence[33] for heavily Mg incorporated samples (Mg concentration of higher than 10^{19} atoms per cm^3). Fig. 1 shows the PL spectra of samples with different concentrations of Mg incorporation (see Table 1). The PL intensities of samples B, C, D and E are shown relative to that of pristine GaN NwN (sample A). We observed significant changes in the luminescence spectra of Mg incorporated films in comparison to that of pristine NwN. The near band edge (NBE) is dominant in samples A, B and C and its intensity increases with increasing Mg : Ga flux. However, in samples D and E, a broad blue luminescence is the dominant emission. Thus, we believe samples B and C are moderately doped, whereas samples D and E are heavily Mg doped GaN NwN. We recorded a 2 and 3.25 times increase in PL intensity for samples B and C, respectively, w.r.t. sample A. An increase in PL intensity at lower Mg incorporation has previously been attributed to the screening of the polarization induced field by Mg,[37] which enables efficient overlapping of e–h wave functions, resulting in a higher recombination probability. However, samples D and E, which were grown at higher Mg flux, have their NBE intensity significantly quenched while the intensity of the broad blue luminescence peaks increase. We note that in sample C, unlike in samples A and B, a shoulder peak is observed at ≈ 3.2 eV. The peak in this vicinity is usually attributed to donor–acceptor pair (DAP) luminescence originating either from the transition from a shallow donor level to a shallow acceptor level or due to a Mg–H complex.[38] It is widely observed experimentally,[39] and estimated theoretically,[40] that the Mg in GaN creates a shallow transient state with a transition energy of 0.15–0.26 eV above VBM. In the present case, the difference between the NBE and the corresponding peak falls within the range of the above mentioned values. Since the films were grown using N$_2$ plasma MBE, the formation of the Mg–H complex is less probable, we attributed this shoulder peak to the DAP transition.

Table 1 Mg flux rate

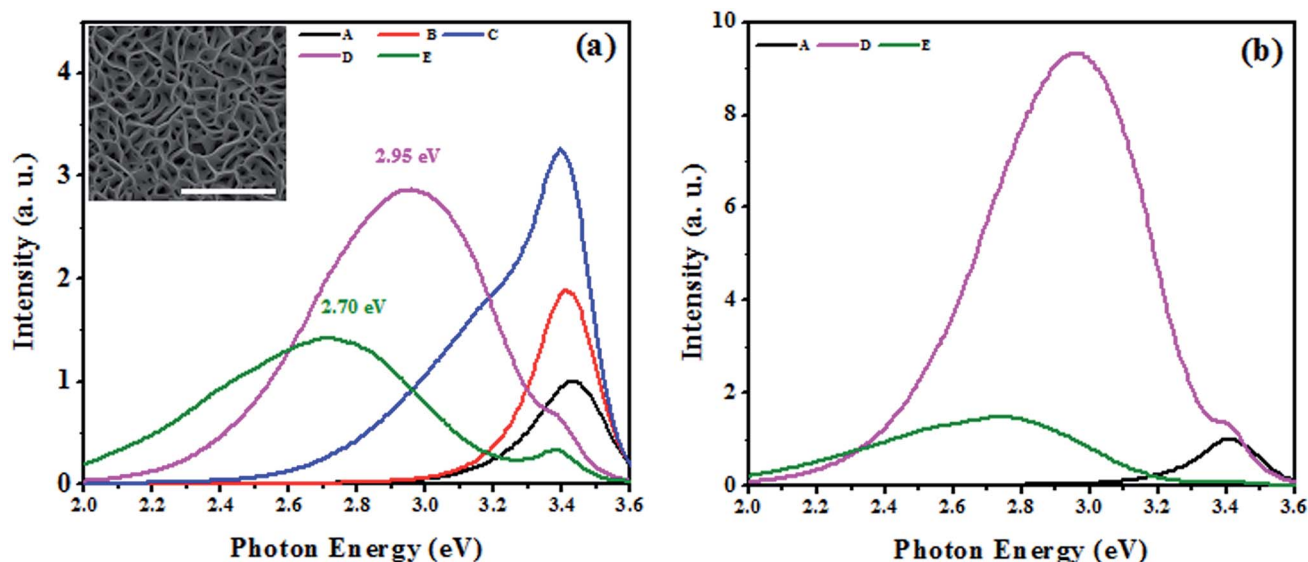| Sample name	Mg-K cell temp (°C)	BEP (Torr)	Flux (atoms per cm^2 per s)	Mg : Ga
A	—	—	—	0
B	300	2.9×10^{-10}	8.6×10^{-10}	0.0017
C	320	7.1×10^{-9}	2.0×10^{12}	0.0393
D	340	1.1×10^{-8}	3.1×10^{12}	0.0622
E	360	2.0×10^{-8}	5.6×10^{12}	0.1102

Fig. 1 (a) shows room temperature photoluminescence (RT-PL) spectra of the undoped and Mg incorporated GaN NwN samples. The inset in the figure shows the SEM image of sample E with a scale bar of 500 nm. (b) shows the PL spectra of samples D and E after annealing at 800 °C in the presence of N_2 for 20 minutes. (Note that the PL spectrum of sample A shown in (b) is obtained without annealing the sample.)

In the cases of samples grown at higher Mg flux (D and E); we observed reduced intensity of NBE emission from the Mg incorporated GaN NwN. In the case of sample D, the peak at 2.95 eV was dominant and a reduced NBE appeared at 3.4 eV. For sample E, the NBE emission was further diminished and a broad peak at 2.7 eV became dominant. The origin of such blue luminescence peaks has been highly debated[39] while some recent experimental[35,41] and Density Functional Theory (DFT)[42,43] studies suggest some understanding. Usually, the 2.9 eV peak appears in heavily Mg doped GaN and is regarded as the signature of Mg doped GaN.[35] While Kaufmann et al.[44] attributed this peak to the transition from a deep donor state to a shallow acceptor state, where the deep donor state is due to the formation of vacancy complex $Mg_{Ga}V_N$, Akasaki et al.[45] attributed this peak to the transition from hydrogen-related deep donor states to Mg acceptor states. Some reports suggest that the blue luminescence (2.7–2.95 eV) is due to the transition from Conduction Band Minimum (CBM) to the deep acceptor state, which appears due to hole localization.[40] It has been proposed theoretically that[40,42] the relaxation patterns (local strain behaviours) of neutral and charged Mg_{Ga} configurations are different from each other, which results in the creation of a deep acceptor state, 0.54 eV above the Mg_{Ga} related shallow acceptor state, which lies 260 meV above the bulk VBM. The appearance of this peak confirms the incorporation of Mg in GaN. It can be clearly seen from the PL spectra (see Fig. 1) that the blue luminescence peak is intense and broad. The cause of broadening in such luminescence peaks can be understood from the configuration co-ordinate diagram presented by Reshchikov et al.[33] and Van de Walle et al.,[40] who estimated that the energy difference between the blue luminescence peaks and the zero phonon line is around 0.54 eV, which can also result in the broadening of blue luminescence peaks in PL spectra. Thus, the peaks observed at 3.43, 3.42, 3.41, 3.40 and 3.39 eV are

attributed as the NBE for undoped GaN and Mg incorporated GaN by using a Mg flux of 8.6×10^{10}, 2.0×10^{12}, 3.1×10^{12} and 5.6×10^{12} atoms $cm^{-2} s^{-1}$, respectively. The results suggest that Mg incorporation in GaN yields a red-shift in the NBE, which is consistent with earlier reports.[46]

To study the impact of thermal treatment on the blue luminescence of Mg incorporated GaN, we annealed samples D and E at 800 °C for 20 minutes in the presence of N_2. The PL spectra (see Fig. 1(b)) of the annealed samples showed a large increase in the intensity of the 2.95 eV peak (for sample D), whereas the intensity of the 2.7 eV peak (for sample E) did not change significantly, which indicates that the origins of these luminescence peaks is different. The increase in the intensity of the blue luminescence is due to increased activation of incorporated Mg atoms as acceptors because of the high temperature annealing and results in more acceptor recombination centers that are responsible for the DAP transition.[47] It is speculated that a complex of substitutional Mg and nitrogen vacancies ($Mg_{Ga}V_N$) is responsible for the deep donor state.[47] However, the blue luminescence at 2.95 eV is enhanced by thermal annealing, whereas the concentration of the ($Mg_{Ga}V_N$) complex significantly decreases after annealing at $T > 500$ °C,[48] which suggests that the origin of the blue luminescence is not from the $Mg_{Ga}V_N$ complex. Different defect complexes of substitutional Mg and interstitial Mg that are formed with increasing Mg flux may cause the 2.7 eV peak, which was recently found to be compensating the donors in Mg doped GaN.[27] The appearance of blue luminescence in Mg incorporated GaN also suggests that the Mg concentration[47] in GaN is higher than 10^{20} atoms per cm^3 in the case of samples D and E.

To study the impact of Mg incorporation on the local strain in the grown films, the local vibrational modes (LVMs) were monitored by Raman spectroscopy and are shown in Fig. 2. The LVM of Mg doped GaN[34,36] appears at ≈ 657 cm^{-1}. As Mg replaces
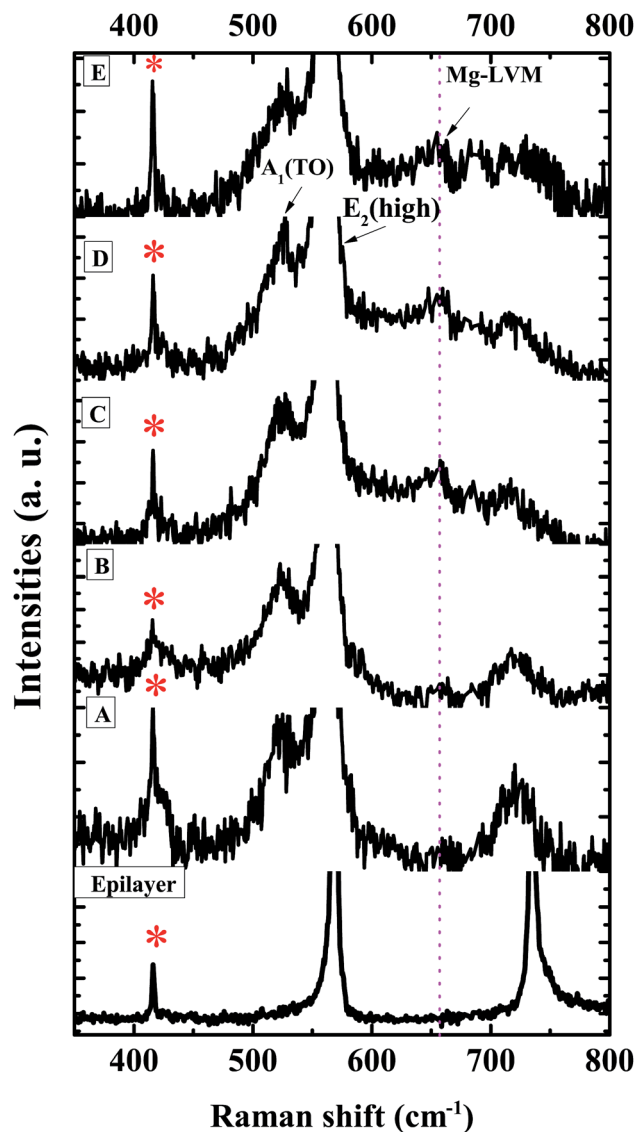
Fig. 2 Raman spectra of the samples studied here. "*" represents the phonon mode from sapphire. The appearance of Mg related LVM can be seen with an increase in Mg : Ga flux. The dotted line is drawn at 657 cm^{-1} to ease visualisation.

Fig. 3 (A–D) represent the NBE, FWHM of the Raman E_2(high) mode, position of the Raman E_2(high) mode and XRD rocking curve of (0002) and (1011) reflex as a function of Mg flux (or Mg : Ga).

Ga, compressive strain is introduced which shifts the E_2(high) mode towards higher energies. The E_2(high) mode, being a non-polar mode, is suitable for the study of in-plane strain.[36] To observe morphology induced changes, we have also plotted the Raman spectrum of a flat 3 μm thick GaN epilayer on c-sapphire. Along with the allowed modes, two geometrically forbidden modes such as E_1(TO) and A_1(TO) are observed in all of the GaN NwN samples, due to scattering off the sidewalls of the porous structure.[20,49] We can clearly observe the presence of the LVM at 657 cm^{-1} in Fig. 2, which is due to the Mg–N stretching mode. The LVM peak is absent for both the GaN epilayer and undoped NwN, but increases with higher Mg flux. The variation of position and Full width at half maximum (FWHM) of the E_2(high) mode with Mg flux, as well as the Mg to Ga ratio for all of the studied samples, is shown in Fig. 3. As it can be seen, the position of the
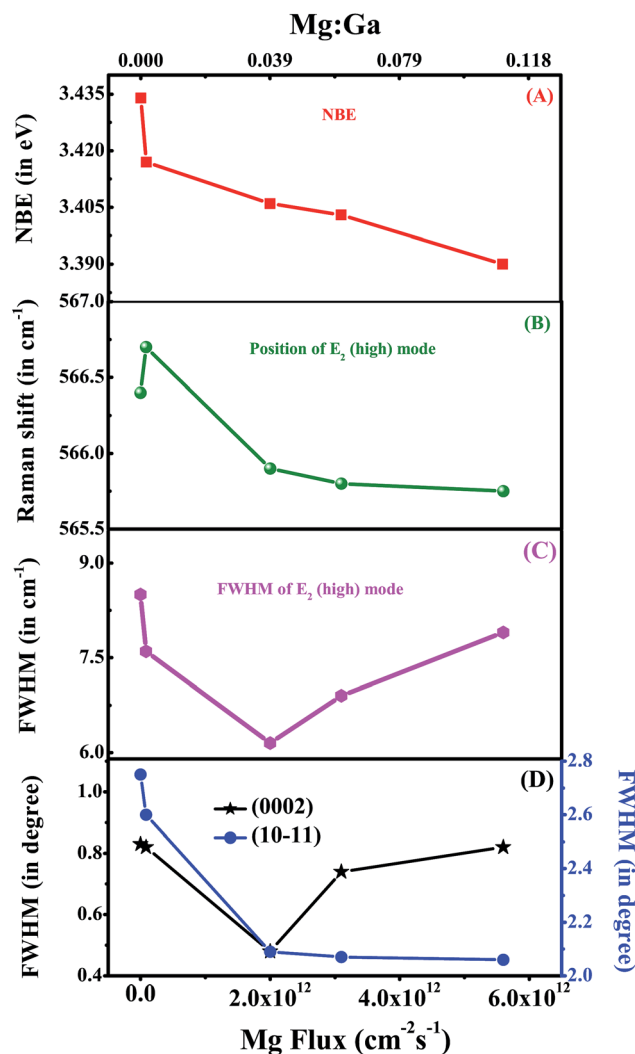
E_2(high) mode for sample B shifts towards higher energy, as expected, but for other samples this mode shifts towards lower energy. As Mg in GaN usually induces compressive strain because of its higher ionic radius, the E_2(high) mode shifts towards high frequency. However, if defect complexes or different charged states other than Mg_{Ga}^0, such as Mg_{Ga}^-, are formed then the phonon frequency shifts to lower energy, due to the developed tensile strain in the structure.[34] The FWHM of the E_2(high) mode shows a large change from the highest value of 8.5 cm^{-1} in GaN NwN to 7.6, 5.6, 7.2, and 7.9 cm^{-1} for samples B, C, D and E, respectively, due to the generation of different defects[34] in the films depending on Mg incorporation.

Strain is introduced in the system not only by Mg replacing Ga in the lattice, but also due to the formation of point and extended defects and impurity complexes, which can also modify the lattice parameters.[34,50] To study the impact of Mg incorporation in the crystal structure of the NwN, a HR-XRD study has been carried out. We recorded both 2θ–Ω and ω-

scans (rocking curve (RC)) of the (0002) and (10$\bar{1}$1) reflexes, which provide information about the stress and crystal quality of the samples, respectively. We compare the acquired results with those of an undoped GaN NwN. We have reported earlier[20] that the undoped GaN NwN possesses very low strain compared to a flat epitaxial thin film. For the Mg incorporated GaN NwN we observed complex strain behaviour. The estimated (c) lattice parameters from HR-XRD for samples A, B, C, D and E are 3.1714 (5.1915), 3.1983 (5.1926), 3.2004 (5.1913), 3.2017 (5.1909) and 3.1801 (5.1956) Å, respectively. The FWHM of the RC of the (0002) and (10$\bar{1}$1) reflexes for the samples are shown in Fig. 3(D). The FWHM of the RC of (0002) displays "U" type behavior with increasing Mg : Ga flux, whereas for (10$\bar{1}$1), the values reduce as Mg incorporation increases. The broadening of the XRD peaks in the NwN is mainly due to the mosaicity that arises due to the misalignment of the nanowalls, as reported earlier.[21,51] Thus, these observations suggest that Mg incorporation reduces mosaicity in films.

We have performed XPS measurements on samples A, C, D and E to study the variation in electronic structure and also to find the composition of Mg in sample E. Fig. 4(A) and (B) represents the Ga-3d and N-1s core level spectra of sample A, whereas (C), (D) and the inset in (E) represent the Ga-3d, N-1s and Mg-2p core level spectra of sample E, respectively (for samples C and D refer to Fig. 3 in the ESI†). All of the core level peaks were deconvoluted and are shown in the same figure to identify the different constituent peaks. For sample A (undoped GaN), the Ga-3d peak is found to consist of a single peak, centered at 20.38 eV and originates from Ga–N bonding. The deconvoluted N-1s core level shows three different peaks centered at 397.89, 395.65 and 393.25 eV (see Table 2). The peak centered at 397.89 eV is assigned to the binding energy of N due to bonding with Ga, whereas the other two peaks are identified as results of Ga Auger LMM transitions.[29]

For sample E, we have observed that Ga-3d and N-1s core levels are broad and red-shifted compared to those of sample A. The deconvolution of the Ga-3d peak for sample E (see Fig. 4(C)) indicates the appearance of two peaks centered at 20.38 and 19.05 eV. The peak centered at the lower binding energy is due to the change in local chemical and structural properties around the Ga atoms due to Mg incorporation. The deconvoluted N-1s core levels (see Fig. 4(D)) show four different peaks, of which the peak corresponding to N–Ga bonding is red shifted by 0.76 eV, compared to the undoped sample (sample A). The origin of the other two peaks centered at 395.65 and 393.25 eV are Ga Auger LMM transitions, as already discussed. For sample E, the large red shift of the E$_2$(high) mode and its broadening, as observed in the Raman study, correlates to the defect complex formation within the film.[34,36] Now, we have observed the appearance of a small peak centered at 391 eV in the N-1s core level for E (and also in the case of C and D), which we believe is due to the defect complex formation during epitaxial growth.

From Table 2, it is clear that the binding energy of the Ga-3d and N-1s core levels of samples with increased Mg : Ga ratios, are red shifted compared to A, which suggests that a continuous downward shift of the Fermi level towards VBM occurs with increasing Mg concentration.[52] In order to study the position of
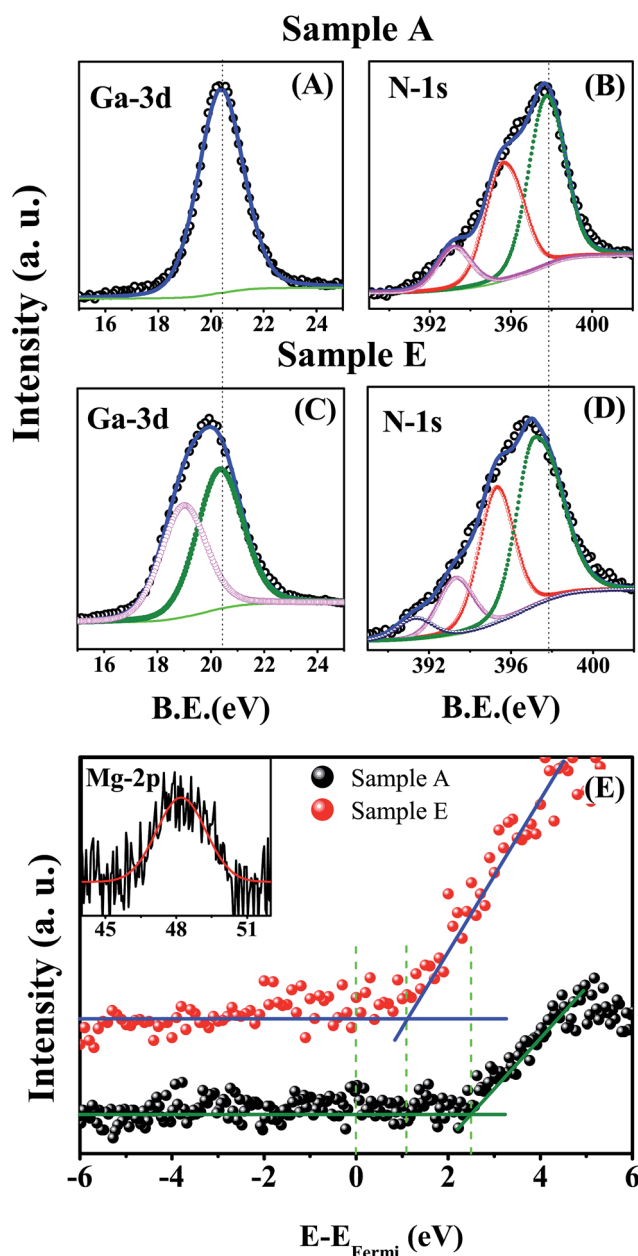

Fig. 4 (A) and (B) show Ga-3d and N-1s core level spectra of the undoped GaN NwN (sample A). (C)−(E) represent the Ga-3d, N-1s core level and valence band spectra of the Mg incorporated GaN NwN (sample E). The inset in (E) shows the Mg-2p core levels. The green line in the core levels is the Shirley background.

the Fermi level in comparison to VBM, we have analyzed the valence band spectra of samples A, C, D and E, and the results are tabulated in Table 2. Fig. 4(E) shows the valence band spectra of samples A and E (the valence band and core level spectra of samples C and D are given in Fig. 3 the ESI†). We have noted that with increasing Mg concentration, the difference between the Fermi level and VBM ($E_F - E_{VBM}$) reduces. The difference ($E_F - E_{VBM}$) for the undoped sample (A) is 2.45 eV, which indicates n-type character, while for samples C, D and E the values are 2.20, 1.82 and 1.09 eV, respectively. This indicates

Table 2 XPS data

Mg : Ga	Ga-3d peak position (in eV)	FWHM of Ga-3d peak (in eV)	N-1s peak position (in eV)	$E_{Fermi} - E_{VBM}$ (in eV)
0.0000 (A)	20.38	2.03	397.89	2.45
0.0017 (B)	—	—	—	—
0.0393 (C)	20.25	2.03	397.60	2.20
0.0622 (D)	19.90	2.57	397.51	1.84
0.1102 (E)	19.85	2.64	397.13	1.09

a transition from an n- to p-type GaN NwN, due to the increase in Mg dopant concentration. As the RT band gap of the GaN NwN is ≈ 3.4 eV, $E_F - E_{VBM}$ should be ≤ 1.7 eV to have p-character and thus we conclude that the transition from n-type to p-type occurs when Mg : Ga is higher than 0.0622. We have further estimated the amount of Mg incorporation in sample E using the following equation

$$C_{Mg}(\%) = \frac{I_{Mg}/ASF_{Mg}}{\sum I_i/ASF_i} \times 100$$

where, C_{Mg}, I_{Mg} and ASF_{Mg} represent the fraction of Mg, intensity of the Mg-2p peak and its atomic sensitivity factor, while I_i and ASF_i are the intensity and atomic sensitivity factors of the other constituent elements (i), respectively. We have used atomic sensitivity factors for Ga-2p$_{3/2}$, N-1s and Mg-2p as 3.720, 0.477 and 0.120, respectively. The estimated value of Mg incorporation in sample E is $\approx 3.3\%$, which corresponds to a Mg atomic concentration of $\approx 9 \times 10^{20}$ cm^{-3} and is quite consistent with our predictions from PL measurements.

Furthermore, to understand the elemental distribution profile, we carried out SIMS measurements on all of the samples as shown in Fig. 5. As discussed earlier, Mg is observed to segregate on the surface in Mg doped flat GaN thin films.[28–31] Our results (see Fig. 5) show that Mg segregates at the surface of the NwN and also at the GaN/Al$_2$O$_3$ interface for samples D and

E. For heavily Mg incorporated sample E, Mg accumulates more at the interface. However, the depth profile of Mg in samples B and C shows Mg segregation only at the surface and decreases monotonically. To further verify that this profile is not due to the unique geometry of the NwN, we recorded N and Ga depth profiles for all of the samples and it was found that the depth profile remains almost constant along the depth. As a typical case, the N and Ga depth profile of sample D is presented in the inset of Fig. 5. The profile shows a fairly constant Ga and N distribution along the depth.

It has been proposed theoretically that Mg incorporation is easier on a Ga-polar surface than on a N-polar surface[53] and also such doping can change the polarity of the film from Ga-polar to N-polar.[53,54] Convergence Beam Electron Diffraction (CBED) measurements (not shown here) on the un-doped GaN NwN confirm that the pristine GaN NwN is Ga-polar in nature. Thus, at the initial stage of growth Mg incorporation is higher, while with increasing growth time a change in polarity of the crystal occurs, and may be the cause for the lower incorporation of Mg. We observed that the Mg concentration in the films towards the interface is 1.6 and 1.9 times higher compared to that at the surface for the samples D and E, respectively. Furthermore, a close inspection of the SIMS spectra of samples B and C shows a change in SIMS signal by an order of magnitude from the surface to the bulk region, while for samples D and E the changes are small (≈ 2 times). This confirms that the concentration of Mg in the bulk is of the same order of magnitude as surface Mg concentration in sample D and E.

The optical signature of GaN NwN : Mg indicates that the Mg atoms occupy Ga sites in the GaN NwN, which results in the DAP transition, centered at 3.2 eV for lower incorporation of Mg. On the other hand, for higher Mg incorporation, the luminescence spectra are observed to be dominated by blue luminescence, whose origin is still widely debated in the literature. A Raman study, along with HR-XRD analysis of the grown samples, suggests that upon moderate incorporation of Mg in the GaN NwN structure, the mosaicity of the film is reduced. A detailed XPS study reveals that, with an increase in the Mg concentration, Ga-3d and N-1s core levels are red shifted and broadened. The broadening of Ga-3d is attributed to the de-localized nature of the hole, generated by Mg incorporation. The difference between the Fermi-level and valence band edge consistently decreases with increasing Mg concentration. Further SIMS data analysis shows that the concentration of Mg in the bulk of the films is of the same order of magnitude as that on the surface. Thus, the entire material has uniform Mg incorporation and
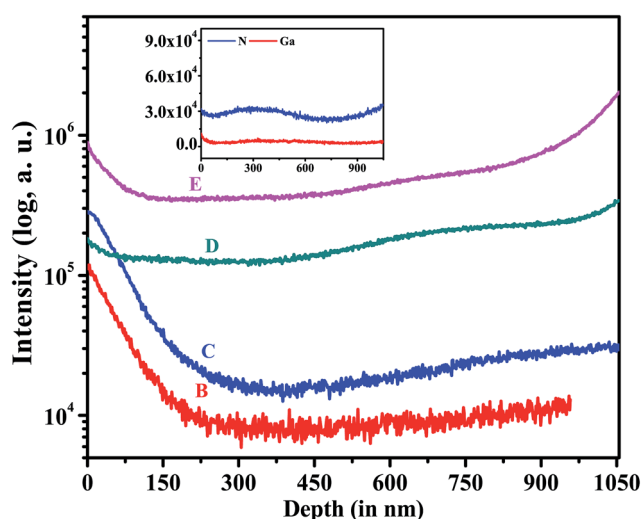

Fig. 5 The depth profile of Mg as a function of depth. The inset of the figure shows the depth profile for Ga and N in sample D.

can open up a new route to obtain efficient p-GaN with a high amount of Mg incorporation.

4 Conclusions

In conclusion, we have studied the structural, optical and electronic properties and dopant distribution in Mg-incorporated GaN NwNs. We have found a 3.2 times enhancement in the NBE for samples with low Mg flux (Mg : Ga < 0.04), while higher Mg flux (Mg : Ga > 0.06) appreciably reduces the NBE and increases blue luminescence. Thermal annealing in the presence of N_2 increases the intensity of blue luminescence (2.95 eV), whereas it does not affect the 2.7 eV peak. We have observed that, with increasing Mg : Ga flux, the E_2(high) vibrational mode shifts towards lower frequency, indicating a change in local strain from the compressive to the tensile type. XPS revealed that more than 10^{20} cm^{-3} of Mg atoms can be incorporated in the sample while retaining its NBE, due to its unique morphology with very high surface to volume ratio. XPS valence band spectra show the transition from n-type to p-type with increasing Mg incorporation. Higher light extraction capability, along with higher incorporation of Mg, in the NwN morphology suggests that these GaN films can be used to fabricate p-type GaN for GaN/InGaN based quantum well structures for LEDs and LDs, with enhanced efficiency.

Acknowledgements

References

1 R. D. Dupuis, M. R. Krames and S. Member, *J. Lightwave Technol.*, 2008, **26**, 1154–1171.
2 S. T. Sheppard, K. Doverspike, W. L. Pribble, S. T. Allen, J. W. Palmour, L. T. Kehias and T. J. Jenkins, *IEEE Electron Device Lett.*, 1999, **20**, 161–163.
3 T. C. Lu, T. T. Kao, S. W. Chen, C. C. Kao, H. C. Kuo and S. C. Wang, *Appl. Phys. Lett.*, 2008, **92**, 141102.
4 T. Sasaki, S. Sonoda, Y. Yamamoto, K. I. Suga, S. Shimizu, K. Kindo and H. Hori, *J. Appl. Phys.*, 2002, **91**, 7911.
5 J. K. Sheu, C. C. Yang, S. J. Tu, K. H. Chang, M. L. Lee, W. C. Lai and L. C. Peng, *IEEE Electron Device Lett.*, 2009, **30**, 225–227.
6 Y. Kuwahara, T. Fujii, Y. Fujiyama, T. Sugiyama, M. Iwaya, T. Takeuchi, S. Kamiyama, I. Akasaki and H. Amano, *Appl. Phys. Express*, 2010, **3**, 111001.
7 D. Wang, A. Pierre, M. G. Kibria, K. Cui, X. Han, K. H. Bevan, H. Guo, S. Paradis, A. R. Hakima and Z. Mi, *Nano Lett.*, 2011, **11**, 2353–2357.
8 S. J. Pearton, B. S. Kang, S. Kim, F. Ren, B. P. Gila, C. R. Abernathy, J. Lin and S. N. G. Chu, *J. Phys.: Condens. Matter*, 2004, **16**, R961–R994.
9 J.-L. Muraro, G. Nicolas, D. M. Nhut, S. Forestier, S. Rochette, O. Vendier, D. Langrez, J.-L. Cazaux and M. Feudale, *Int. J Microw. Wirel. T.*, 2010, **2**, 121.
10 S. Miwa, Y. Kamo, Y. Kittaka, T. Yamasaki, Y. Tsukahara, T. Tanii, M. Kohno, S. Goto and A. Shima, *IEEE MTT-S International, Microwave Symposium Digest (MTT)*, 2011, pp. 1–4.
11 T. Kuykendall, P. Ulrich, S. Aloni and P. Yang, *Nat. Mater.*, 2007, **6**, 951–956.
12 S. Pimputkar, J. S. Speck, S. P. DenBaars and S. Nakamura, *Nat. Photonics*, 2009, **3**, 180–182.
13 C. Wiesmann, K. Bergenek, N. Linder and U. T. Schwarz, *Laser Photonics Rev.*, 2009, **3**, 262–286.
14 H. W. Choi, M. D. Dawson, P. R. Edwards and R. W. Martin, *Appl. Phys. Lett.*, 2003, **83**, 4483–4485.
15 A. David, H. Benisty and C. Weisbuch, *J. Disp. Technol.*, 2007, **3**, 133.
16 O. V. Bilousov, J. J. Carvajal, H. Geaney, V. Z. Zubialevich, P. J. Parbrook, O. Mart, J. Jime, D. Francesc, M. Aguilo and C. O. Dwyer, *ACS Appl. Mater. Interfaces*, 2014, **6**, 17954.
17 C. B. Soh, C. B. Tay, R. J. N. Tan, A. P. Vajpeyi, I. P. Seetoh, K. K. Ansah-Antwi and S. J. Chua, *J. Phys. D: Appl. Phys.*, 2013, **46**, 365102.
18 C. C. Yang, C. F. Lin, C. M. Lin, C. C. Chang, K. T. Chen, J. F. Chien and C. Y. Chang, *Appl. Phys. Lett.*, 2008, **93**, 2006–2009.
19 M. Kesaria, S. Shetty, P. Cohen and S. Shivaprasad, *Mater. Res. Bull.*, 2011, **46**, 1811–1813.
20 V. Thakur, S. K. Nayak, K. K. Nagaraja and S. M. Shivaprasad, *Electron. Mater. Lett.*, 2015, **11**, 398–403.
21 S. K. Nayak, D. Shamoon, J. Ghatak and S. M. Shivaprasad, *Phys. Status Solidi A*, 2017, **214**, 1600300.
22 M. Zhang, P. Bhattacharya, W. Guo and A. Banerjee, *Appl. Phys. Lett.*, 2010, **96**, 132103.
23 E. Cimpoiasu, E. Stern, R. Klie, R. a. Munden, G. Cheng and M. a. Reed, *Nanotechnology*, 2006, **17**, 5735–5739.
24 A. J. Ptak, L. J. Holbert, L. Ting, C. H. Swartz, M. Moldovan, N. C. Giles, T. H. Myers, P. Van Lierde, C. Tian, R. A. Hockett, S. Mitha, A. E. Wickenden, D. D. Koleske and R. L. Henry, *Appl. Phys. Lett.*, 2001, **79**, 2740–2742.
25 S. M. Myers, A. F. Wright, G. A. Petersen, W. R. Wampler, C. H. Seager, M. H. Crawford and J. Han, *J. Appl. Phys.*, 2001, **89**, 3195–3202.
26 I. P. Smorchkova, E. Haus, B. Heying, P. Kozodoy, P. Fini, J. P. Ibbetson, S. Keller, S. P. DenBaars, J. S. Speck and U. K. Mishra, *Appl. Phys. Lett.*, 2000, **76**, 718.
27 G. Miceli and A. Pasquarello, *Phys. Rev. B: Condens. Matter Mater. Phys.*, 2016, **93**, 165207.
28 Y. Nakano and T. Jimbo, *Phys. Status Solidi C*, 2002, **442**, 438–442.
29 T. Hashizume, *J. Appl. Phys.*, 2003, **94**, 431.
30 T. Cheng, S. Novikov, C. Foxon and J. Orton, *Solid State Commun.*, 1999, **109**, 439–443.
31 L. T. Romano, M. Kneissl, J. E. Northrup, C. G. Van De Walle and D. W. Treat, *Appl. Phys. Lett.*, 2001, **79**, 2734–2736.
32 M. Kesaria and S. M. Shivaprasad, *Appl. Phys. Lett.*, 2011, **99**, 143105.

33 M. A. Reshchikov, D. O. Demchenko, J. D. McNamara, S. Fernández-Garrido and R. Calarco, *Phys. Rev. B: Condens. Matter Mater. Phys.*, 2014, **90**, 035207.

34 R. Kirste, M. P. Hoffmann, J. Tweedie, Z. Bryan, G. Callsen, T. Kure, C. Nenstiel, M. R. Wagner, R. Collazo, A. Hoffmann and Z. Sitar, *J. Appl. Phys.*, 2013, **113**, 103504.

35 O. Gelhausen, M. Phillips, E. Goldys, T. Paskova, B. Monemar, M. Strassburg and A. Hoffmann, *Phys. Rev. B: Condens. Matter Mater. Phys.*, 2004, **69**, 125210.

36 H. Harima, *J. Phys.: Condens. Matter*, 2002, **14**, R967–R993.

37 N. Zhang, Z. Liu, Z. Si, P. Ren, X.-D. Wang, X.-X. Feng, P. Dong, C.-X. Du, S.-X. Zhu, B.-L. Fu, H.-X. Lu, J.-M. Li and J.-X. Wang, *Chin. Phys. Lett.*, 2013, **30**, 087101.

38 M. Reshchikov, G.-C. Yi and B. Wessels, *Phys. Rev. B: Condens. Matter Mater. Phys.*, 1999, **59**, 13176–13183.

39 B. Monemar, P. P. Paskov, G. Pozina, C. Hemmingsson, J. P. Bergman, S. Khromov, V. N. Izyumskaya, V. Avrutin, X. Li, H. Morkoc, H. Amano, M. Iwaya and I. Akasaki, *J. Appl. Phys.*, 2014, **115**, 053507.

40 L. Lyons, A. Janotti and C. G. V. D. Walle, *Phys. Rev. Lett.*, 2012, **108**, 156403.

41 U. Kaufmann, M. Kunzer, M. Maier, H. Obloh, A. Ramakrishnan, B. Santic and P. Schlotter, *Appl. Phys. Lett.*, 1998, **72**, 1326–1328.

42 Q. Yan, A. Janotti, M. Scheffler, C. G. V. D. Walle, Q. Yan, A. Janotti, M. Scheffler and C. G. V. D. Walle, *Appl. Phys. Lett.*, 2012, **100**, 142110.

43 J. Buckeridge, C. R. A. Catlow, D. O. Scanlon, T. Keal, P. Sherwood, M. Miskufova, A. Walsh, S. M. Woodley and A. A. Sokol, *Phys. Rev. Lett.*, 2015, **114**, 016405.

44 U. Kaufmann, M. Kunzer, H. Obloh, M. Maier, C. Manz, A. Ramakrishnan and B. Santic, *Phys. Rev. B: Condens. Matter Mater. Phys.*, 1999, **59**, 5561–5567.

45 Y. Koide, D. E. Walker, B. D. White, L. J. Brillson, M. Murakami, S. Kamiyama, H. Amano and I. Akasaki, *J. Appl. Phys.*, 2002, **92**, 3657–3661.

46 Y.-P. Sui and G.-H. Yu, *Chin. Phys. Lett.*, 2011, **28**, 067807.

47 M. A. Reshchikov and H. Morkoİğc, *J. Appl. Phys.*, 2005, **97**, 061301.

48 S. Hautakangas, K. Saarinen, L. Liszkay, J. A. Freitas and R. L. Henry, *Phys. Rev. B: Condens. Matter Mater. Phys.*, 2005, **72**, 165303.

49 T. L. Williamson, D. J. DÄśİĄaz, P. W. Bohn and R. J. Molnar, *J. Vac. Sci. Technol., B: Microelectron. Nanometer Struct.– Process., Meas., Phenom.*, 2004, **22**, 925.

50 M. A. Moram and M. E. Vickers, *Rep. Prog. Phys.*, 2009, **72**, 036502.

51 D. Poppitz, A. Lotnyk, J. W. Gerlach and B. Rauschenbach, *Acta Mater.*, 2014, **65**, 98–105.

52 S. R. Ryu, S. D. G. Ram, S. J. Lee, H.-d. Cho, S. Lee, T. W. Kang, S. Kwon, W. Yang, S. Shin and Y. Woo, *Appl. Surf. Sci.*, 2015, **347**, 793.

53 Q. Sun, A. Selloni, T. H. Myers and W. A. Doolittle, *Phys. Rev. B: Condens. Matter Mater. Phys.*, 2006, **73**, 155337.

54 L. Romano, J. Northrup, A. Ptak and T. Myers, *Appl. Phys. Lett.*, 2000, **77**, 2479.